Ad hoc radiometric calibration of a thermal-infrared camera

Stephen Vidas
SAIVT Laboratory
QUT Science and Engineering Faculty
Email: stephen.vidas@qut.edu.au

Peyman Moghadam
Autonomous Systems Laboratory
CSIRO Computational Informatics
Email: peyman.moghadam@csiro.au

***Abstract*—Many applications can benefit from the accurate surface temperature estimates that can be made using a passive thermal-infrared camera. However, the process of radiometric calibration which enables this can be both expensive and time consuming. An ad hoc approach for performing radiometric calibration is proposed which does not require specialized equipment and can be completed in a fraction of the time of the conventional method. The proposed approach utilizes the mechanical properties of the camera to estimate scene temperatures automatically, and uses these target temperatures to model the effect of sensor temperature on the digital output. A comparison with a conventional approach using a blackbody radiation source shows that the accuracy of the method is sufficient for many tasks requiring temperature estimation. Furthermore, a novel visualization method is proposed for displaying the radiometrically calibrated images to human operators. The representation employs an intuitive coloring scheme and allows the viewer to perceive a large variety of temperatures accurately.**

I. Introduction

Thermal-infrared cameras are an effective and increasingly popular tool for many computer vision and image processing applications such as search and rescue [3] and energy auditing [18]. In addition to a robustness to difficult lighting and atmospheric conditions [4], they also provide the ability to estimate surface temperature [13]. However, as a prerequisite for performing quantitative temperature estimation, the cameras must regularly go through a process of radiometric calibration.

Radiometric calibration is a procedure that models the relationship, which varies with sensor temperature, between the digital output of the camera and the incident radiation. Determining the level of incident radiation can then enable accurate temperature estimates to be made, which can enhance the utility of the images for tasks such as object recognition and segmentation. The conventional calibration process is time consuming, and requires expertise and access to expensive equipment to achieve good results. The option of periodically returning the camera to the vendor for re-calibration may be further complicated by export restrictions that affect many thermal-infrared models.

This paper presents an adhoc radiometric calibration method which can be performed in under 2 hours and requires no specialized equipment. The method is appropriate for applications for which the accuracy requirements may not justify the costs or effort associated with alternative approaches. The proposed approach is evaluated against a standard approach using an expensive thermal blackbody, and results show that it achieves comparable accuracy for a range of typical target temperatures.

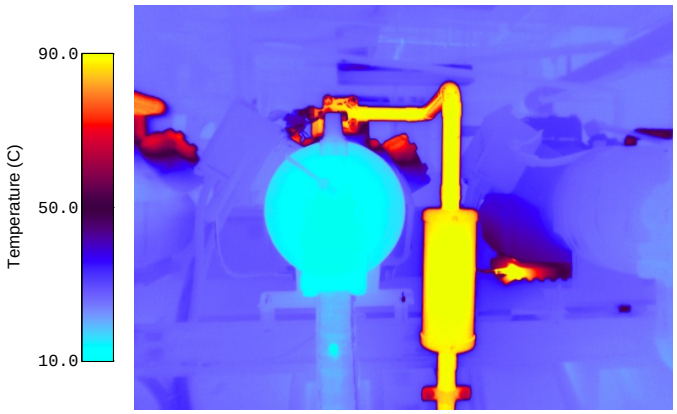

Fig. 1: An image radiometrically calibrated and colorized using the two proposed methods. The image depicts an industrial HVAC system containing components both below and well above ambient temperature.

For visualizing the radiometrically corrected images, an intuitive color mapping scheme named "Perceptive" is proposed. This visualization method achieves both a high level of discernability between temperature levels, and an intuitive appearance. Its design is based on the principals of perceptual balance inherent in the CIELUV colorspace, and so it avoids problems common to many popular schemes that may mislead the viewer into over or underestimating temperature differences.

Figure 1 shows an image radiometrically calibrated using the proposed calibration method, with the proposed visualization applied. Software implementations for both the proposed adhoc calibration method and the proposed visualization scheme are available at the project website.[1]

II. Background

This section will first discuss relevant operating characteristics of thermal-infrared cameras, before providing a brief review of the areas of thermal-infrared radiometric camera calibration, and the visualization of radiometrically corrected thermal-infrared images.

[1] http://code.google.com/p/thermalvis-ros-pkg/

A. Operating Characteristics

Common microbolometer thermal-infrared cameras contain a Focal Plane Array (FPA) of elements sensitive to long-wave infrared radiation. As each pixel in the FPA is excited by the incident radiation, its resistance is altered, which in turn varies its output voltage. This voltage is ultimately quantized to become the raw image digital pixel value, but this has been shown to depend on a number of factors beyond simply the incident thermal-infrared radiation [15]. Many of these factors are fixed properties of the imaging sensor such as the integration time, the Temperature Coefficient of Resistance (TCR), and the integration capacitance. However, a significant property which influences the voltage is the existing sensor temperature, which can vary due to factors such as the ambient temperature, the time since the device was powered on, and the historical incident radiation [15]. Generally thermal-infrared cameras will contain at least one thermistor (temperature measuring element) attached to the imaging sensor, which can be used to track the sensor temperature as image data is captured.

Along with sensor and target temperature, the raw digital output of thermal-infrared cameras is also greatly affected by the presence of spatial non-uniformities, producing a phenomenon known as Fixed Pattern Noise (FPN). This form of noise is caused by small but unavoidable differences in the responsivity of the individual bolometer pixels. These are largely due to inconsistencies in the materials and manufacturing process, but can be exacerbated by environmental effects.

The problem of FPN is made more complex by the fact that non-uniformities vary over time, and therefore a single static model of the noise is not adequate to fully account for its effect [14]. In order to accurately recover the thermal-infrared signal by accounting for FPN, a combination of a once-off initial offline modelling step and ongoing real-time adjustments are used. These forms of image correction are not to be confused with the process of radiometric calibration that is the major focus of this paper.

In order to correct image noise in real-time, an internal shutter within the camera housing is intermittently closed in what is commonly referred to as a Non-Uniformity Correction (NUC) or Flat-Field Correction (FFC). This has the negative affect of interrupting the data output of the camera, but allows the gain and offset for each pixel to be updated using an assumption of uniform temperature across the internal shutter [7]. This mechanical behaviour of the camera was exploited for the proposed method, as discussed in Section IV.

B. Radiometric Calibration

While thermal-infrared cameras do not directly measure temperature, they do sense incident irradiance which is directly related to target surface temperature. Forming a model which accounts for the behaviour of the camera under different conditions is what is referred to as radiometric calibration [1]. Without radiometric calibration the usefulness of thermal-infrared cameras is limited to applications which have no need for temperature estimation. However, even tasks which conventionally do not utilize temperature as a distinctive characteristic of object surfaces may benefit from this knowledge, as it allows strict constraints to be introduced for classification and feature extraction purposes.

Brightness temperature is a value that is used to describe the equivalent surface temperature that would produce a specific digital output value from a thermal-infrared camera, under ideal environment conditions. This intuitive representation of the thermal-infrared image data is often preferred over more scientifically precise representations such as incident radiation power, and is referred to throughout the paper.

The automatic execution of an internal NUC within a conventional thermal-infrared camera effectively eliminates the independent characteristics of each pixel, so that for calibration the multi-pixel image can be treated as a single measurement, provided that it views a surface of uniform temperature and uniform radiation properties [5].

The method of [9] presents a calibration approach involving a blackbody source and an environmental chamber (a temperature controlled environment). A blackbody is an idealized entity that absorbs all incident Electro-Magnetic (EM) radiation, and whose emitted radiation is purely a function of its temperature alone. Given the assumption of a perfect blackbody, the Stefan-Boltzmann law states that its irradiance or emissive power $j*$ is proportional to the fourth power of the blackbody's temperature T, as shown in Equation 1.

$$j* = \sigma T^4 \tag{1}$$

Whilst no perfect blackbody exists, objects that behave sufficiently like a blackbody for practical purposes have been manufactured and are a popular tool for thermal-infrared camera calibration.

For the aforementioned method [9], the temperature of the blackbody target was varied from between 10 and 50 degrees, in steps of 10 degrees, over a period of 14 hours. Simultaneously, the chamber temperature was oscillated between 10 and 30 degrees, which in turn caused the internal camera temperature to vary between approximately 21 and 28 degrees throughout the experiment. The reason for the smooth oscillation was to ensure that the internal temperatures remained coupled to the Focal Plane Array (FPA) temperature, which was the only internal temperature able to be measured during camera operation. Using recorded data, the behavioral properties both independent and dependent of FPA temperature were able to be modelled for each pixel. Results were then able to be applied directly on the raw output of the camera to achieve temperature stabilized images.

The works of [10] and [11] follow similar principals, but instead use heated targets made of specialized materials painted in high emissivity paint, and with several attached thermocouples, as an alternative to a blackbody source. Other methods which avoid the use of such equipment nevertheless require prior temperature estimates to be made, in contrast to the proposed approach [12].

C. Thermal-infrared Visualization

The effective visualization of radiometrically corrected thermal-infrared images can significantly enhance their utility. The naive way for monochromatic thermal-infrared images

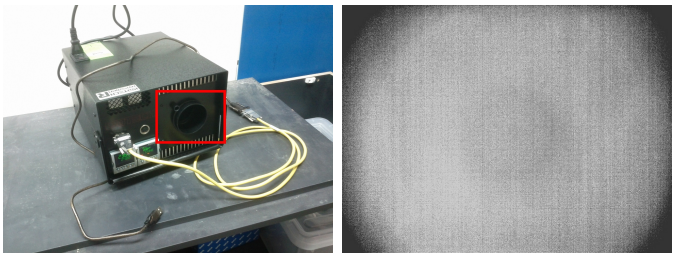

(a) Observer Viewpoint (b) Camera Viewpoint

Fig. 2: Images of the blackbody source. The model used was the Isotech 982 Hyperion. The tubular cavity (highlighted in red) contains the temperature-controlled blackbody surface itself, and the camera is mounted so that its view is fully occupied by this surface. The image from the camera viewpoint after mounting has been significantly intensity-scaled for visualization purposes because it has a very low graylevel range due to the highly uniform temperature of the target surface.

to be displayed is in grayscale form by simply scaling the temperatures to range between black (cold) and white (hot). However, humans can typically perceive only around 100 different shades of grey, and are capable of perceiving many times more different colors, so the colorization of images can therefore enhance a user's ability to extract information [16]. The process of false-color mapping the grayscale thermal image to a color representation is often accompanied by a colorbar to help the viewer associate pixel RGB values with temperature estimates.

Many thermal-infrared cameras are sold with accompanying operation software which provides a variety of false color palettes that can be applied to the default grayscale output of the camera in real-time. The most popular schemes surveyed were those referred to as "rainbow" schemes, which map colors of the rainbow to grayscale intensity, and "iron" schemes, which assign the naturally changing color states of iron as it is heated up to high temperatures. However, these colormaps lack a strong theoretical basis, and as a result can introduce artifacts and discontinuities that mislead the viewer into over or underestimating the magnitude of temperature differences throughout the image [2]. While superior colormaps have been presented in the literature, those found have been generalized schemes that have not been explicitly purposed for thermal-infrared data [6], [8], [20].

III. Blackbody Calibration

To form a baseline for comparison, radiometric calibration of the thermal-infrared camera was performed with the use of a thermal blackbody. The method used was an adaptation of the work of [9] that can function without the need of a temperature-controlled environment [18].

First, a blackbody source (shown in Figure 2) was used in combination with the thermal-infrared camera to obtain all required data.

The proposed methodology for data capture is shown in Algorithm 1. Steps 9 to 14 are fully automated. The result of the data capture algorithm is a large number of images with corresponding target and sensor temperature information, that can be used to generate the radiometric model. For the experiments, target temperatures between 10 and 50 degrees in increments of 10 degrees were explored.

Algorithm 1 Data Capture Procedure for Blackbody Radiometric Calibration

1: Determine range and resolution of sample temperatures.
2: Power-up blackbody and connect to computer.
3: Position camera so that full field-of-view is covered by blackbody target.
4: **for** $t_{BB} \leftarrow t_{min} : t_{max}$ **do** ▷ t_{BB}: blackbody temp.
5: Set blackbody temperature to (t_{BB}).
6: Wait for blackbody temperature to stabilize.
7: Wait for camera to cool.
8: Power up camera.
9: **while** Camera is heating up **do**
10: Perform a NUC (Non-Uniformity Correction).
11: Immediately record an image.
12: Record the thermal sensor (thermistor) temperature.
13: Record the blackbody source temperature.
14: **end while**
15: Switch camera off.
16: **end for**

The procedure for generating the radiometric model from the captured blackbody data first involved reducing the data into a collection of individual samples each corresponding to a single image. Each of these samples contains the mean image value (digital output), instantaneous sensor temperature and instantaneous blackbody temperature. It was assumed that this information would be sufficient for the model, which attempts to determine a mapping $f()$ from sensor temperature (T_S) and digital pixel graylevel (G) to target temperature (T_T), as shown in Equation 2.

$$T_T = f\left(T_S, G\right) \tag{2}$$

Next, samples which are likely to represent highly transient states of the camera were discarded. It was assumed that in a steady-state, the graylevel should increase as the camera heats up. That is, an increase in voltage would be expected for a fixed irradiant power as the internal temperature increases the resistance. Therefore, transient samples were defined as those that occurred while the image graylevels were decreasing.

Finally, the relationship between the image graylevel, sensor temperature and blackbody target temperature was modeled using multiple linear regression. This relationship is shown in Equation 3, where T_T is the blackbody target temperature, T_S is the sensor (thermistor) temperature and G is the pixel graylevel.

$$\begin{aligned} T_T = &-(7.71 \times 10^2) + (7.15 \times 10^0)T_S + (2.00 \times 10^{-1})G \\ &- (1.20 \times 10^{-1})T_S^2 - (1.30 \times 10^{-5})G^2 \end{aligned} \tag{3}$$

The second-order regression model achieved an R-squared value of 0.9996. The model can be interpretted as a mapping

between pairs of digital pixel graylevels and sensor temperatures, and blackbody target temperature. Equation 1 can be used to convert T_T from the brightness temperature to a sensed radiance, which then allows an environment model to be applied in order to achieve a surface temperature estimate.

IV. Ad hoc approach

The proposed ad hoc calibration method can be applied to a regular uncooled microbolometer thermal-infrared camera, provided that it contains the common features of a readable thermistor and a controllable shutter. For the experiments, an open-source driver for operating the camera and its associated features using the linux operating system was employed.[1]

The calibration procedure requires some manual preparation, prior to the completely automated capture of a single data sequence, which can then be used to generate a radiometric model. The control, data streaming and processing associated with this fully automated procedure has been implemented in the Robotics Operating System (ROS) and OCTAVE. The full process is shown in Algorithm 2.

Algorithm 2 Data Capture Procedure for Ad Hoc Radiometric Calibration

```
Stabilize environment
Power-up camera
Start recording from camera
while Camera is heating up do
    Close shutter
    Perform a NUC (Non-Uniformity Correction)
    Capture frame and record thermistor reading
    Open shutter
    Perform a NUC (Non-Uniformity Correction)
    Capture frame and record thermistor reading
end while
Switch camera off.
```

A. Scene Preparation

For the proposed calibration approach, the camera was rigidly positioned to face a static scene for approximately 60 minutes, while the camera heated up. The scene must be physically static (having no physical motion), as well as having no change in temperature. Best results were achieved with a variety of constant surface temperatures in view, such as the example shown in Figure 3, which includes cool background surfaces at ambient temperature, a warmer computer monitor displaying a static image, and a desktop lamp which contains surface temperatures ranging from moderate to very hot. Practically, there is no benefit in having surface tempeatures in view that are beyond the range of temperatures that the device itself will experience as it is heated up, which would typically not be less than 24 degrees or exceed 44 degrees Celsius. Other useful objects may include devices or power supplies which are on standby.

All powered devices were turned on for 10 minutes before the procedure was started to ensure that the scene was in steady-state - that is, that temperatures would stay constant as data was recorded. In addition, the air-conditioning was maintained at a constant ambient temperature.

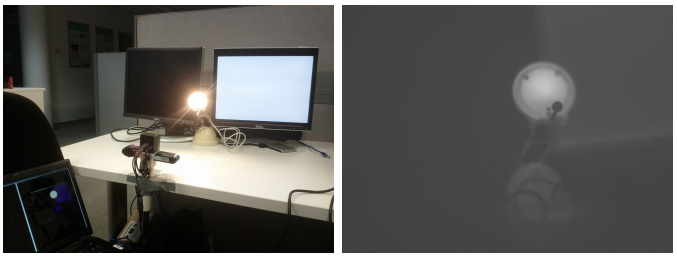

(a) Observer viewpoint (b) Camera viewpoint

Fig. 3: Example scene used for ad hoc radiometric calibration. This thermal-infrared image includes objects of a range of temperatures, enabling the radiometric model to be generalized over the full range of sensor temperatures explored.

Reflective (low-emissivity) surfaces were avoided for the experiment, however, these are not necessarily a problem provided that the backgrounds that are reflected also remain at a constant temperature for the duration of data capture.

For preparing the camera itself, it was left unpowered for several hours so that it began at ambient temperature. The case of the camera was wrapped in plastic for the duration of data capture in order to accelerate the natural process of heating, and increase the maximum temperature of the camera achieved at the end of the sequence. Other methods for further increasing the maximum temperature such as using active heating elements may be possible, however, it is crucial that the position of the camera is not disturbed, and that the temperatures in the viewed scene are not influenced by such a method. If it is possible to cool the camera below ambient temperature safely before capturing data, this will in turn extend the valid range of the resulting model.

B. Data Capture

Once the scene has been set up, data capture can be performed. For the experiment, the process of recording data took approximately 60 minutes.

Throughout the sequence, the camera shutter was alternately closed and opened at 5 second intervals. For each captured frame, the sensor temperature from the termistor was also recorded. NUC operations were performed for every 0.05 degree increase in sensor temperature to reduce noise in the readings.

The resulting data from this process consist of a collection of both open- and closed-shutter images, with corresponding thermistor measurements. The next section (Subsection IV-C) outlines how this data was used to form a radiometric model.

C. Model Generation

When the open and close shutter commands are sent to the camera, there is no way to know the number of frames that are received during the delay before the change in shutter state occurs. In addition, sometimes the opening and closing of the shutter can corrupt a small numbers of frames. Therefore, an image analysis approach was developed to classify all frames

in the captured data sequence as either open-shutter, closed-shutter, or corrupted.

This image analysis approach begins with the assumption that open-shutter images have a much larger range of pixel intensities than the closed shutter images. For each new image, if the intensity range was consistent with that of the last open-shutter image, it was defined as an open-shutter image. This consistency was defined using a threshold cue determined through empirical analysis - the image must have a graylevel intensity range a maximum of 100 levels less than the most recently classified open-shutter image. Similarly, the consistency criteria empirically determined for closed-shutter images was having a graylevel intensity range of no more than 50 greater than the previous closed-shutter image. Any images which failed to meet either of these conditions were classified as corrupted. Manual inspection verified that all open-shutter and closed-shutter images were correctly classified using this method, and the overwhelming majority of corrupted images were also classified correctly.

Given the closed-shutter images determined using this approach, the principal assumption exploited was that these images provide a view of a uniform-temperature surface (the inside of the shutter), with the the thermistor reading at that instant of time giving an accurate indication of the surface temperature of the viewed surface. Therefore, for a range of thermistor temperatures, the gray level corresponding to a surface of the same temperature was known.

A 3D curve (the spine) was then formed by interpolating this data, which enabled the equivalent graylevel corresponding to a surface temperature equal to the temperature of the thermistor to be known for any temperature in between the lowest and highest thermistor readings. This curve was used to predict what the graylevel representing a surface of the same temperature as the camera should be for any open shutter frame.

Each open-shutter image was then inspected in order to find such pixels - that is, those that were situated on the spine (having a graylevel indicating that it represents a surface of the same temperature as the current thermistor temperature). This way, an estimate can be made of the temperature for all surfaces in the scene that have a temperature within the range of thermistor temperatures explored (i.e. those that are modelled by the initial curve). This resulted in a large number of pixels throughout the open-shutter sequence having corresponding temperature estimates.

For each surface temperature for which a corresponding pixel was found, all pixels in a single image representing that same surface temperature were segmented. Then, for each frame, the average graylevel of all pixels in each group was associated with the estimated surface temperature, and the thermistor temperature, to form a 3D point (comprised of graylevel, thermistor temperature and target temperature) for use in generating the model. However, similarly to the blackbody approach, all images for which the camera was in its highly-transient state (again assuming the period of decreasing median graylevel represents the transient state) were disregarded for this step.

Multiple linear regression was then used to fit a model to these points (in the same way as in Section III), which was intended to accurately represent the mapping for all temperatures (surface or target, and thermistor) within the range of $max(T_a, T_x)$ to $min(T_b, T_y)$. Here T_a and T_b are the starting (minimum) and ending (maximum) temperatures of the thermistor for the calibration sequence, and T_x and T_y are the minimum and maximum temperatures of surfaces in the scene used for calibration. The model is shown in Equation 4, where T_T is the target "Brightness" temperature, T_S is the sensor (thermistor) temperature and G is the pixel graylevel.

$$T_T = -(5.96 \times 10^2) + (9.68 \times 10^0)T_S + (1.17 \times 10^{-1})G - (1.67 \times 10^{-1})T_S^2 - (4.74 \times 10^{-6})G^2 \quad (4)$$

The second-order regression model achieved an R-squared value of 0.97731. The total time required to generate the model upon completion of data capture was approximately 60 minutes.

V. Ad hoc evaluation

The thermal-infrared camera used for the experiments was a Thermoteknix Miricle 307K. It has a spatial resolution of 640×480 pixels, and a pixel depth of 14 bits. It is typical of thermal-infrared cameras used for computer vision and robotics, in utilizing an FPA of uncooled microbolometers as the sensing element.

The evaluation is divided into two parts. First, models generated using both the blackbody (Section III) and ad hoc (Section IV) approaches are assessed for accuracy in estimating surface temperatures. Second, the ad hoc model is directly compared with the blackbody model under the demonstrated assumption that the blackbody model can act as a reliable form of ground truth.

A. Accuracy

The first experiment involved testing the models on video footage of the blackbody source set to a variety of temperatures. Figure 4 shows the error in estimated target temperature achieved using both models over the full range of tested sensor operating temperatures (approximately 26.0 to 43.0 degrees Celsius). It can be seen that within a range of typical target temperatures (10.0 to 50.0 degrees Celsius) the ad hoc model achieves accuracy of within 2.0 degrees, which is inferior but comparable with the blackbody approach, which achieves accuracy of within 0.6 degrees across this range.

A further experiment tested the ability of the models to estimate the temperature of practical targets. Three cups of water were filled with cold (10.7 C), room-temperature (23.1 C) and hot (54.4 C) water respectively. Figure 5 shows the estimates achieved using the two approaches with the ad hoc estimates on top and the blackbody estimates beneath.

The surface temperature estimates achieved using the two methods differ from the temperature of the water as measured using a more accurate contact temperature probe. However, this is likely due to the real difference in temperature between the surface and the body of the water, due to heat transfer between the air and the water across this interface. More importantly, the estimates achieved using the two methods were very similar.

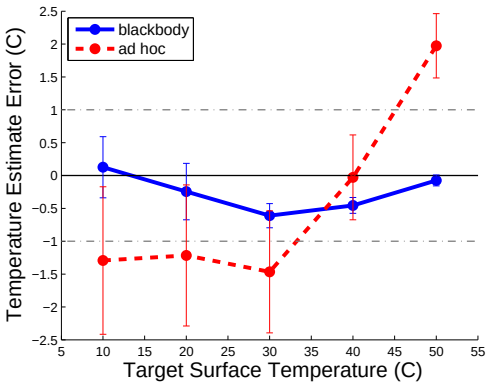

Fig. 4: Accuracy of both the ad hoc and standard blackbody models. Error bars show one standard deviation of variation from the mean error.

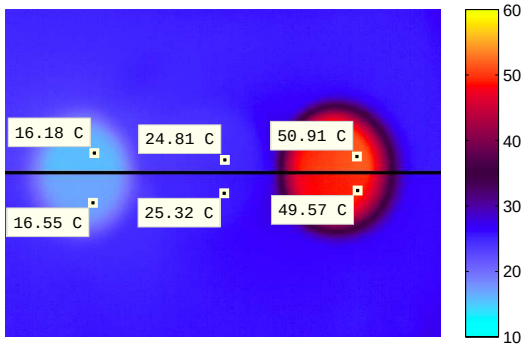

Fig. 5: Water surface temperature estimates using the ad hoc model (top) and the blackbody model (below).

B. *Difference between models*

In the previous section, the blackbody model was demonstrated to accurately estimate target temperatures within 0.6 degrees over a large range of thermistor and target temperatures, and therefore can be assumed to be a reliable form of ground truth. Figure 6 shows the difference in estimated target temperature for the two models across the full valid range of the blackbody model. The average difference between the models is 1.25 degrees Celsius, with a maximum difference of 3.65 degrees. While this accuracy of the ad hoc approach may not be sufficient for applications such as medical thermography, it is nevertheless sufficient for many applications where accuracy requirements may not warrant an investment in expensive equipment such as a thermal blackbody. In any case, it is comparable with the quoted accuracies of many commercially available thermal-infrared cameras, which often only claim to estimate temperature accurate to within 2 or even 5 degrees.

VI. Visualization Method

Once a thermal-infrared camera has been radiometrically calibrated using the proposed method, images captured from the device can be displayed to viewers with a corresponding colorbar. This colorbar conveys the connection between pixel intensity or RGB value, and target temperature.

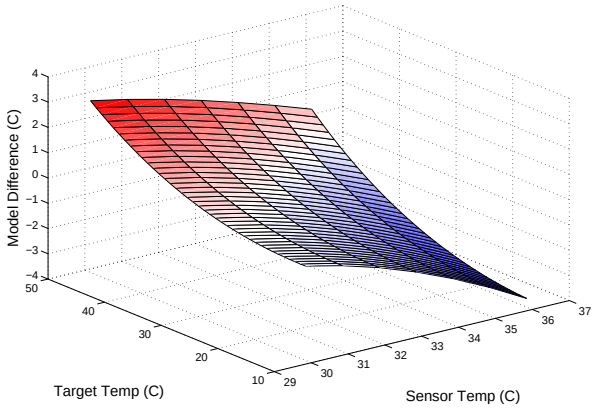

Fig. 6: Ad hoc radiometric calibration model error. The red portion of the curve represents where the ad hoc model predicts higher temperature than the blackbody model, and the blue region represents the opposite.

Existing colormapping schemes that are well established conventions for visualizing thermal-infrared images lack a strong theoretical basis. A common problem with these schemes is that equal differences in temperature are not represented by equal perceptual differences in color, and as a result the viewer may be misled into thinking objects have a temperature difference greater or less than their true difference. A new colormapping scheme is proposed that achieves signficantly better perceptual balance based on the principals of the CIE 1976 LUV color space. In designing this colormapping method, the following major ideal properties were pursued:

- easy discernibility between temperature levels
- an intuitive association between color and relative temperature
- perceptual balance

In addition to perceptual uniformity, this thermal-infrared false-color pallete, “Perceptive”, is designed to portray more temperature resolution than a grayscale representation, whilst maintaining an intuitive appearance. Its effectiveness is demonstrated in Figure 7 where it is used to colorize the same scene shown in Figure 3b.

A key goal of the CIE 1976 LUV standard (shown in Figure 8) is to achieve perceptual uniformity, that is, an equal distance in the color space should correspond to an equal difference in color from the perspective of a typical human. This property was exploited for the development of the proposed mapping, where colors were sampled from CIELUV from approximately equally spaced positions (numbered 1 through 11). This results in temperature differences of the same magnitude being equally distinguishable by a viewer, regardless of where the temperatures fall on the color scale. The ordering of the samples followed similar pattern to that of the rather intuitive “Iron” colorbar, but it was extended with icy colors to represent colder temperatures - thereby effectively

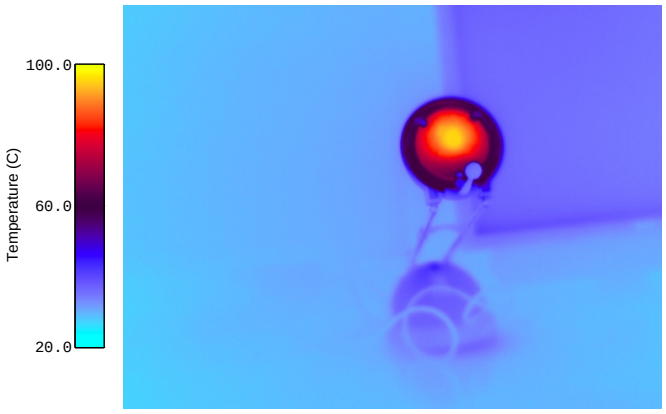

(a) Camera viewpoint

Fig. 7: Radiometrically corrected and colorized version of image shown in Figure 3b.

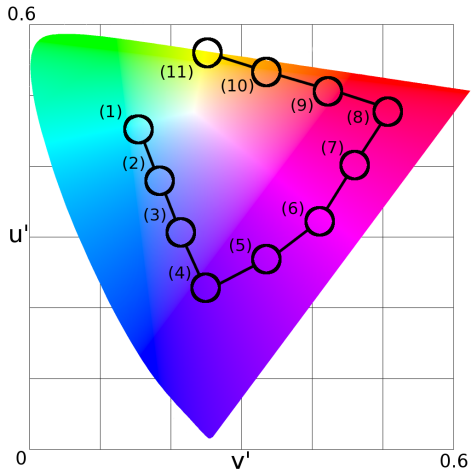

Fig. 8: The CIELUV standard color space. The proposed colormap was formed by sampling colors in the order of the labeled points, and then smoothly varying RGB values between these samples. Samples near certain edges of the space were avoided, as most computers cannot portray color differences in these regions.

increasing the number of unique temperatures in the scene that are able to be discerned from a single representation.

From the points sampled in Figure 8, interpolation was used to create a smooth function mapping relative temperature intensities to colors. Then, the lightness of the samples was smoothed linearly in CIELAB colorspace for both the lower half (decreasing) and upper half (increasing) of the range.

Figures 9, 10 and 11 compare the proposed scheme with two popular existing alternatives. While it can be seen that the "Rainbow" colormap conveys a large amount of detail, the colorbar appears to have distinct bands despite representing a smooth range of temperatures. This results in artificial discontinuities in the image that can exaggerate temperature differences between particular pairs of temperatures from the perspective of the viewer. In addition, the nature of the colors is not particularly intuitive, in that it is not clear which surfaces are hotter or colder without referring to the colorbar.

In contrast, the iron colormap has a highly intuitive color scheme which can be understood even without looking at the colorbar, but it lacks the ability to portray as many distinct temperatures. The proposed approach manages to convey a large amount of detail whilst still using intuitive colors, and the colors are varied smoothly to prevent the user from being misled with regard to the magnitude of temperature differences. The images have been undistorted using a calibration method specifically tailored for thermal-infrared cameras [17]. The proposed mapping can equally be applied to 3D temperature models [19].

VII. Conclusion

A novel, ad hoc method for the radiometric calibration of a typical thermal-infrared camera was proposed. The method allows the digital output of the camera to be accurately mapped to a brightness temperature over a typical range of scene and sensor temperatures. Although the extent of the valid range is limited by the safe operating temperatures of the camera, the evaluation has shown that the model can be extrapolated beyond these limits with reasonable accuracy. The proposed method is useful for when cost, time or logistical constraints prohibit the use of conventional blackbody approaches.

A novel visualization method for thermal-infrared images radiometrically calibrated by the ad hoc approach has also been proposed. The visualization scheme combines an intuitive appearance with a facility to discern a high number of distinct temperature levels in the image, and avoids artifacts and discontinuities common to many existing methods.

Acknowledgment

The authors gratefully acknowledge funding of the project by the CSIRO Realtime Perception project, CSIRO Event-Driven Mobile Node project and CSIRO TCP SSN. The institutional support of both CSIRO and QUT is greatly appreciated.

References

[1] P. Bajcsy and R. Kooper, "Integration of data across disparate sensing systems over both time and space to design smart environments," in *Sustainable Radio Frequency Identification Solutions*, 2010, pp. 281–306. 2

[2] D. Borland and R. M. Taylor, "Rainbow color map (still) considered harmful," *Computer Graphics and Applications, IEEE*, vol. 27, no. 2, pp. 14–17, 2007. 3

[3] C. Brunner *et al.*, "Selective combination of visual and thermal imaging for resilient localization in adverse conditions: Day and night, smoke and fire," *Journal of Field Robotics*, May 2013. 1

[4] S. El-Tawab, M. Abuelela, and Y. Gongjun, "Real-time weather notification system using intelligent vehicles and smart sensors," in *Mobile Adhoc and Sensor Systems*, 2009, pp. 627–632. 1

[5] J. D. Kalma, H. Alksnis, and G. P. Laughlin, "Calibration of small infra-red surface temperature transducers," *Agricultural and forest meteorology*, vol. 43, no. 1, pp. 83–98, 1988. 2

[6] G. Kindlmann, E. Reinhard, and S. Creem, "Face-based luminance matching for perceptual colormap generation," in *Visualization, 2002. VIS 2002. IEEE*, 2002, pp. 299–306. 3

[7] A. Kumar, S. Sarkar, and R. P. Agarwal, "Correcting infrared focal plane array sensor non uniformities based upon adaptive filter," 2006, pp. 1537–1540. 2

[8] A. Light and P. J. Bartlein, "The end of the rainbow? color schemes for improved data graphics," *Eos, Transactions American Geophysical Union*, vol. 85, no. 40, pp. 385–391, 2004. 3

(a) Rainbow colormapping (b) Proposed colormapping (c) Iron colormapping

Fig. 9: A comparison of the alternative colormaps applied to an indoor scene with a relatively low temperature range.

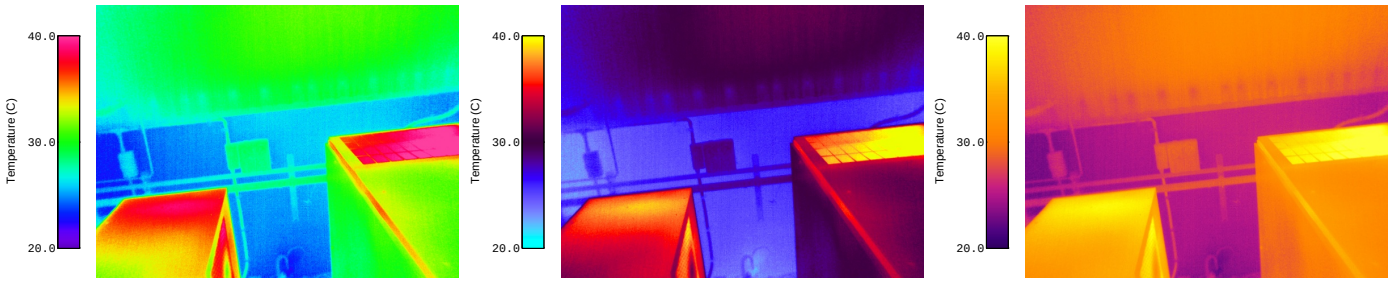

(a) Rainbow colormapping (b) Proposed colormapping (c) Iron colormapping

Fig. 10: A comparison of the alternative colormaps applied to an outdoor industrial scene with a moderate temperature range.

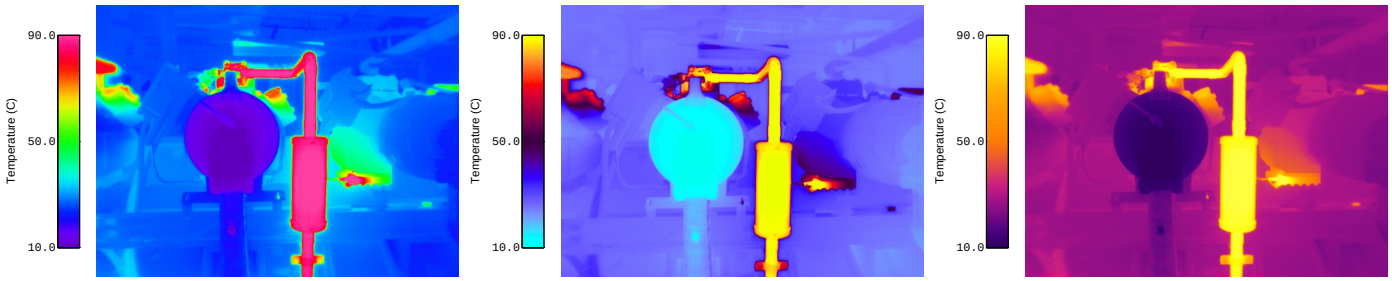

(a) Rainbow colormapping (b) Proposed colormapping (c) Iron colormapping

Fig. 11: A comparison of the alternative colormaps applied to an indoor industrial scene with a large temperature range.

[9] P. Nugent, J. Shaw, and N. Pust, "Correcting for focal-plane-array temperature dependence in microbolometer infrared cameras lacking thermal stabilization," *Optical Engineering*, vol. 52, no. 6, pp. 1–7, 2013. 2, 3

[10] S. Rainieri, F. Bozzoli, and G. Pagliarini, "Characterization of an uncooled infrared thermographic system suitable for the solution of the 2-d inverse heat conduction problem," *Experimental Thermal and Fluid Science*, vol. 32, no. 8, pp. 1492–1498, 2008. 2

[11] S. Rainieri and G. Pagliarini, "Data processing technique applied to the calibration of a high performance FPA infrared camera," *Infrared physics & technology*, vol. 43, no. 6, pp. 345–351, 2002. 2

[12] A. Savelyev and R. Sugumaran, "Surface temperature mapping of the university of northern iowa campus using high resolution thermal infrared aerial imageries," *Remote Sensing of Land Surface Properties, Patterns and Processes*, vol. 8, no. 8, pp. 5055–5068, Aug. 2008. 2

[13] R. Siegel and J. Howell, *Thermal Radiation Heat Transfer*, 4th ed. New York: Taylor and Francis, 2002. 1

[14] S. Sobarzo, J. Pezoa, and S. Torres, "Real-time kalman filtering for nonuniformity correction in infrared focal-plane arrays," *Pattern Recognition, Image Analysis and Applications*, vol. 3773, pp. 752–761, 2004. 2

[15] X. Sui *et al.*, "Response model of resistance-type microbolometer," *Optical review*, vol. 17, no. 6, pp. 525–531, 2010. 2

[16] A. Toet, "Natural colour mapping for multiband nightvision imagery," *Information Fusion*, vol. 4, no. 3, pp. 155–166, 2003. 3

[17] S. Vidas *et al.*, "A mask-based approach for the geometric calibration of thermal-infrared cameras," *IEEE Transactions on Instrumentation and Measurement*, vol. 61, no. 6, pp. 1625–1635, 2012. 7

[18] S. Vidas and P. Moghadam, "HeatWave: a handheld 3D thermography system for energy auditing," *Energy and Buildings*, vol. 66, pp. 445–460, Nov. 2013. 1, 3

[19] S. Vidas, P. Moghadam, and M. Bosse, "3D thermal mapping of building interiors using an RGB-D and thermal camera," in *IEEE International Conference on Robotics and Automation (ICRA)*, 2013, pp. 2303–2310. 7

[20] L. Wang and K. Mueller, "Harmonic colormaps for volume visualization," in *Proceedings of the Fifth Eurographics/IEEE VGTC conference on Point-Based Graphics*, 2008, pp. 33–39. 3